



Observing the dynamic “hot spots” on two-dimensional Au nanoparticles monolayer film†

Cite this: *Chem. Commun.*, 2017, 53, 6788

Received 19th April 2017,
Accepted 23rd May 2017

DOI: 10.1039/c7cc03020g

rsc.li/chemcomm

Chenjie Zhang,^a Enming You,^b Qi Jin,^a Yaxian Yuan,^{*a} Minmin Xu,^a Songyuan Ding,^b Jianlin Yao ^{*a} and Zhongqun Tian^b

Interparticle spacing was controlled by evaporating water on 2D Au nanoparticles arrays. Relationships among SERS effect, SPR catalysis, and gap distance were experimentally and theoretically studied.

Noble metal nanoparticles have attracted considerable interest in many fields because of their unique optical properties known as surface plasmon resonance (SPR), which is due to collective oscillation of free electrons at a dielectric–metal interface under laser irradiation.¹ SPR significantly improves a local electromagnetic field, resulting in a markedly enhanced efficiency of optical processes, and thus has given birth to surface-enhanced infrared absorption spectroscopy (SEIRAS),² surface-enhanced Raman spectroscopy (SERS),³ and surface-enhanced fluorescence spectroscopy (SEFS).⁴ Among them, SERS is one of the most powerful tools for providing remarkably rich vibrational fingerprint information on molecules, up to single molecular sensitivity, inherently originating from coupling of SPR on metal nanostructures.^{5–7} Therefore, a deeper understanding of what triggers the coupling effect is highly desired.

Generally, it is well accepted that SPR could not only play a critical role in the SERS effect, but also exhibit the capability of facilitating some unconventional reactions,⁸ such as the N–N coupling reaction,^{9,10} dissociation of H₂,¹¹ and the decarboxylation reaction.¹² Due to its promising applications in the fields of heterogeneous catalysis and solar energy,¹³ SPR-driven catalytic reactions have aroused great interest. In our previous studies, we demonstrated that a SPR-driven reaction was closely related to plasmon intensity in the nanogaps.¹² Meanwhile, it has already been theoretically and experimentally demonstrated that plasmon intensity is highly dependent on gap distance.^{14,15}

Therefore, controlling interparticle spacing between adjacent nanoparticles with sub-nanometer precision is highly essential in order to maximize the electromagnetic field in a nanogap.¹⁶ In the past decade, many efforts have been made to flexibly adjust and dynamically control gap distance between neighbouring nanoparticles, such as the mechanically controllable break junction method (MCBJ),¹⁷ modulation of temperature¹⁸ and pH,^{19,20} state translation nanoparticle-enhanced Raman spectroscopy (STNERS),²¹ capillarity,²² and magnetically-assisted assembly.²³ Unfortunately, these strategies more or less suffered from a few disadvantages such as, high cost, poor reproducibility, low yield, and structural complexity.¹⁶ Therefore, controlling the spacing of nanoparticles with sub-nanometer precision still remains a great challenge. Additionally, relationships among SERS intensity, catalytic efficiency of SPR, and gap distance need to be clarified for a good understanding of the mechanisms of SERS and surface plasmon reactions.

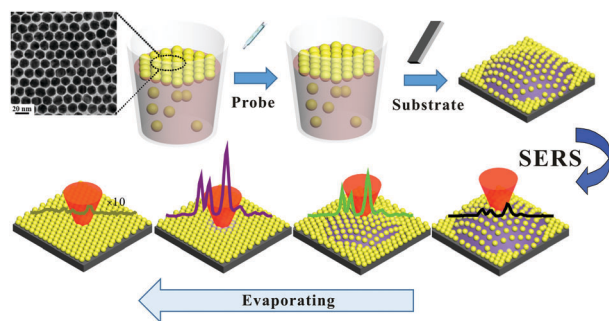
Here, we propose an efficient strategy for dynamic control of interparticle spacing of Au nanoparticles in a two-dimensional (2D) plane. We realized that we could simply evaporate contained water under the Au nanoparticles monolayer film (Au MLF) after transferring it from the air–water interface to a substrate. SERS measurements were performed to study the relationships between the SERS effect, as well as catalytic efficiency of SPR and the gap distance of nanoparticles, *i.e.*, observing dynamic “hot spots.” Theoretical simulation also was carried out to further understand the nature of the dynamic process.

Scheme 1 exhibits the detailed procedure for fabricating dynamic SERS substrates and their corresponding SERS spectra during the water evaporation process. An Au MLF at the air–water interface with a 2D hexagonal close-packed (HCP) structure was obtained (see Fig. S1 and S2, ESI†).²⁴ A clean Si wafer was immersed into the solution at a tilted angle of 5–10° and then pulled out slowly, as a result, the Au MLF deposited tightly onto the surface of the substrate because of its high affinity for the surface. The TEM image of the Au MLF shows that the spacing between Au nanoparticles on a dried substrate was about 1 nm. During the transfer process, the Au MLF was observed to float

^a College of Chemistry, Chemical Engineering and Materials Science, Soochow University, Suzhou 215123, China. E-mail: jlyao@suda.edu.cn

^b State Key Laboratory for Physical Chemistry of Solid Surfaces, College of Chemistry and Chemical Engineering, Collaborative Innovation Centre of Chemistry for Energy Materials (iChEM), Xiamen University, Xiamen 361005, China

† Electronic supplementary information (ESI) available. See DOI: 10.1039/c7cc03020g



Scheme 1 Schematic diagram of the preparation of SERS substrate and SERS measurements during the water evaporation process.

around on the substrate, and a liquid layer was sandwiched between Au nanoparticles and substrate surface due to surface tension.²⁵ During slow evaporation of the liquid layer, the Au nanoparticles were trapped by surface tension which made them strictly confined to the air-water interface on the wafer. Although the total number of Au nanoparticles was unchanged during slow evaporation of the liquid layer, the surface area occupied by Au nanoparticles decreased. Therefore, it was obvious that the spacing between the adjacent Au nanoparticles was reduced by the adhesive force in the evaporation process (as shown in Scheme 1). It is well known that a decrease of interparticle spacing results in an exponential improvement of SERS intensity. Therefore, that qualified it as a promising substrate for observing a change in SERS intensity. To verify this assumption, *in situ* measurements of the arrangement of nanoparticles during evaporation is essential. Unfortunately, conventional electron microscopy techniques cannot be applied to monitor the alterable spacing of a substrate containing water. Generally, a Raman probe also cannot be in such a small gap due to steric hindrance. To eliminate this problem, a drop of Raman probe in ethanol was added to form a self-assembly monolayer on the Au nanoparticles prior to the transfer of Au MLF, continuous time-dependent SERS spectra were acquired immediately.

SERS response during the evaporation process was evaluated by using thiophenol (TP) as a probe due to its well-documented SERS spectral features. Bands at 998, 1078, and 1566 cm^{-1} originated from the in-plane ring deformation mode, in-plane phenyl ring stretching mode, and the C-C stretching mode, respectively.^{26,27} Fig. 1 presents the time-dependent SERS mapping which was performed to monitor the evaporation process. In the initial stage, weak SERS signals of TP were observed due to relatively large interparticle spacing, *i.e.*, a low coupling effect. SERS intensity gradually increased during the evaporation process as anticipated. After about 50 s, the intensity achieved a maximum of about 5 times compared with that at the beginning (Fig. 1C). It should be noted once again that the total number of nanoparticles remained constant because interparticle spacing was regulated in a very small range by the adhesive force between nanoparticles and this was also confirmed by the perfect monolayer structures of the dried Au MLF (as shown in Scheme 1). Moreover, it could also be verified from

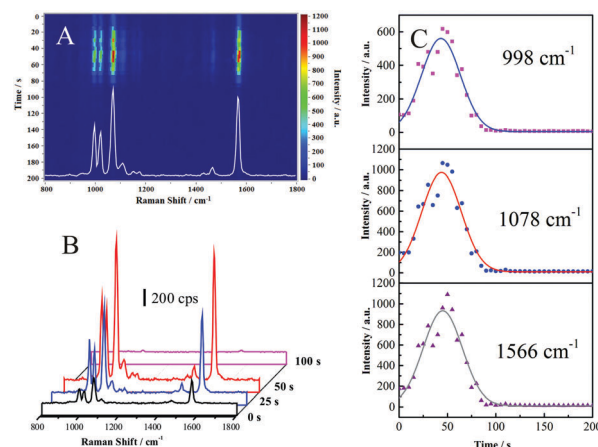


Fig. 1 (A) Time-dependent SERS mapping image of TP adsorbed on Au MLF during the evaporation process. (B) Selected spectra at different states extracted from the mapping data from (A). (C) The corresponding time evolution of Raman intensity at bands of 998, 1078, and 1566 cm^{-1} , respectively.

the microscope images that the colour of Au MLF did not change before the solvent evaporated completely. Accordingly, it is reasonable to assume that the number of probe molecules within the laser spot did not increase further. Thus, the significant increase in SERS intensity could only be attributed to a decrease of the gap distance. In addition, the slowly increasing rate of the TP signals in Fig. 1C illustrate that the spacing between the nanoparticles slowly decreased. Unfortunately, the speed of approaching Au nanoparticles was not constant during the water's evaporation, thus, quantitative analysis of the relationships between SERS intensity, as well as the catalytic efficiency of SPR and gap distance is still a great challenge. However, the possibility of nanoparticles aggregating in the three-dimensional (3D) plane during the evaporation was eliminated. Subsequently, SERS intensity decreased remarkably at about 30 times and then kept constant. This demonstrated that the evaporation was completely finished and all the Au nanoparticles were attached directly onto the substrate. It should be noted that a laser at very low power ($\sim 1.05 \times 10^7 \text{ mW cm}^{-2}$) was used in the present case to avoid attenuation in SERS activity induced by the laser. And the SERS performance of Au MLF is universal for spot-to-spot and sample to sample (Fig. S2 and S3, ESI†).²⁴ Yang and his co-workers reported a similar phenomenon in the change of SERS intensity by using a 3D hot spots matrix formed during evaporation of a droplet of Ag sols.²⁸ The increase in the numbers and activity of "hot spots" contributed to the dramatic improvement of the SERS signal. However, it was still difficult to distinguish each contribution. As mentioned above in our case, the activity of "hot spots" solely contributed to this fact. Therefore, the increase in SERS intensity was associated with the decrease of gap distance in the Au MLF contained water. As the water evaporated, the change in the medium's refractive index and the unfitted SPR frequency caused the dramatic attenuation of the signal.

With the gradual approaching of neighbouring nanoparticles, the intensity of the corresponding electromagnetic field increased

due to the enhanced coupling effect of SPR, *i.e.*, the observation of dynamic “hot spots”. The enhanced electromagnetic field intensity exhibited a bi-function for enhancing Raman signals and triggering the SPR-driven reaction because of the heat effect and hot electrons.⁸ As is well known, *para*-aminothiophenol (PATP) has already become a model molecule for SPR catalytic reactions.⁹ In our present case, PATP was also employed to fill in the gap for observing the effect of gap distance on the SPR-driven reaction. At the beginning of the water evaporation, weak signals at 1070 and 1595 cm^{-1} attributed to a_1 modes of PATP were observed (Fig. 2A). After 25 s, SERS intensity of PATP was twice as strong as in the initial stage (Fig. 2B). This was in good agreement with the experimental fact of TP adsorption with the water-contained Au MLF substrate (as shown in Fig. 1). At the same time, the peaks at 1140, 1388, and 1438 cm^{-1} assigned to the C–N and N=N stretching vibrations of *p,p'*-dimercaptoazobenzene (DMAB) produced from the coupling reaction of PATP, also appeared unambiguously and gradually increased (as shown in Fig. 2B).⁹ It has been previously reported that the transfer of electrons from nanoparticles to $^3\text{O}_2$ became the essential step to accomplish the oxidation of PATP to DMAB. Besides, the photothermal effect induced by SPR also played a critical role.^{29,30} Therefore, absence of the SERS signal from DMAB was mainly contributed by the weak coupling effect of SPR in the initial stage. It should be mentioned that the laser power was kept constant during all the measurements and Au MLF exhibited the SPR catalysis activities with high uniformity (Fig. S4, ESI[†]). It was reasonable to assume that the conversion of PATP to DMAB originated from the change of the SPR effect rather than the laser power. The increased SERS intensity of DMAB thus was attributed to the strong SPR coupling effect in the gap of nanoparticles which was shrunk due to the evaporation of water. As a consequence, that brought enhancement of the electromagnetic field which facilitated the SPR-driven catalytic reaction. After 60 s, the absolute intensity of PATP and DMAB reached the maximum, and the time dependent SERS intensity was comparable to that obtained in the case of TP adsorption (Fig. 1). With the expected attenuation of SERS intensity in the final stage,

the spectral features of DMAB disappeared, demonstrating that the SPR was not enough to cause a catalytic reaction.

It has been reported that DMAB exhibits a_g bands at similar frequencies to those of a_1 modes of PATP (1070 and 1594 cm^{-1}), resulting in an overlap of SERS spectra from PATP and DMAB.⁹ Therefore, it was difficult to distinguish the contributions of PATP and DMAB directly. For convenience, relative intensities of the bands at 1140 cm^{-1} (DMAB) to that at 1070 cm^{-1} (PATP and DMAB) were used to estimate the conversion efficiency from PATP to DMAB.³¹ Fig. 2C presents time-relative Raman intensity of the bands at 1140 cm^{-1} to 1070 cm^{-1} during the evaporation process. This demonstrated the relationship between the catalytic efficiency of SPR and the spacing (gap distance) between the adjacent Au nanoparticles. Although the absolute intensity of PATP and DMAB increased simultaneously at the initial stage of evaporation, the relative intensity almost stayed constant (as shown in Fig. 2C). This was mainly due to the magnification of SERS intensity of PATP and DMAB at the same degree. Therefore, the gap distance did not reach the threshold value for increasing SPR catalyzed conversion. With an extension of evaporation time duration, the relative intensity increased dramatically and reached a maximum at about 60 s. The maximum value of $I_{1140\text{cm}^{-1}}/I_{1070\text{cm}^{-1}}$ of about 1 was comparable to that obtained from pure DMAB adsorbed on Au nanoparticles.³² This indicated that almost all the PATP contributing to the SERS signal was converted into DMAB by the gradually enhanced electromagnetic field during the decrease of the nanoparticle spacing. Generally, high laser power was essential to achieve efficient transformation of PATP.^{29,33,34} However, in the present case, low laser power brought extremely high coupling efficiency. Due to the irreversible reaction of PATP to DMAB, the test area was shifted to another spot to observe the continuous change of SERS intensity with evaporation duration. The relative intensity was close to zero, suggesting the absence of SPR catalyzed conversion.

The maximum relative intensity with a decrease in nanoparticle spacing is extremely sensitive for such low laser power which was not triggered by the conversion reaction. Therefore, in order to highlight the advantage of our strategy for the dynamic control of gap distance, further experiments were performed as comparison, including hot spots controlled in a 3D plane²⁸ and conventional Au nanoaggregates under a dry state. Here, laser power was controlled to inhibit the occurrence of SPR conversion from PATP to DMAB on dried Au nanoparticle nanoaggregates (Fig. S5, ESI[†]). The catalytic efficiency of wetted 3D plane and 2D “hot spots” was much higher than with dried Au nanoaggregates (Fig. 2D). Moreover, the relative intensities were less than 1 in all previous reports involving the conversion of PATP, *i.e.*, the absolute intensity of DMAB at 1140 cm^{-1} was weaker than the combined band at 1070 cm^{-1} . Therefore, observation of spectral features of pure DMAB suggested that almost all the PATP molecules in the gap were converted into DMAB,³² and the contribution of PATP to the SERS signal was quite low beyond the gap area. This also provided a convincing explanation that the SPR catalyzed reaction was locally confined to the “hot spot” area.

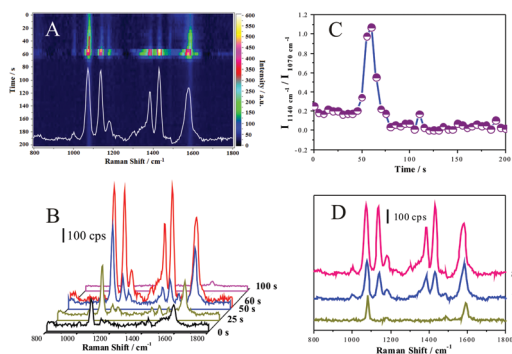


Fig. 2 (A) Time-dependent SERS mapping of PATP on Au MLF during the evaporation. (B) Spectra extracted from the mapping image. (C) Time-relative Raman intensity profile of bands at 1140 cm^{-1} to 1070 cm^{-1} . (D) The difference of catalytic efficiency among (a) dynamic control of gap distance in a 2D plane; (b) a droplet of Au nanoparticles sol during the evaporation process; and (c) dried Au nanoaggregates.

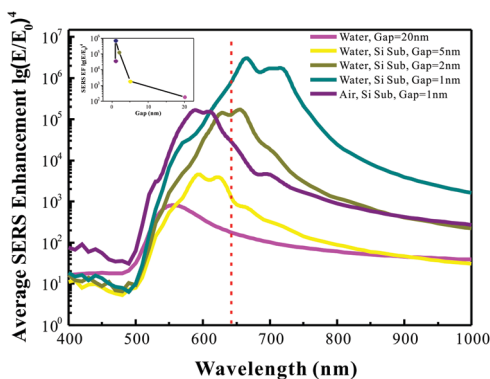


Fig. 3 Theoretical simulation distribution of the average SERS EF in the wavelength range from 400 nm to 1000 nm with the change of the gap distance from 20 nm to 1 nm.

To quantitatively clarify gap distance-dependent SERS activity during the evaporation process, theoretical simulation was explored to systematically investigate the relationship between the SERS enhancement factor (EF) and gap distance of the adjacent Au nanoparticles (details of theoretical simulations are given in ESI†). As shown in Fig. 3, the EF value continued increasing with the decrease of spacing from 20 nm to 1 nm. Most importantly, the frequencies of SPR peaks slightly redshifted for matching with proper excitation wavelength; the SERS EF decayed nearly 2 orders of magnitude and the SPR frequency blue shifted because of the change of the medium's refractive index from water ($n \approx 1.33$) to air ($n \approx 1$). With combined SERS features and theoretical simulation, it was assumed that change of the distance between adjacent nanoparticles was at a scale of nanometer or sub-nanometer. It should be noted that the interspacing of nanoparticles remained constant after the contained water was completely evaporated. Decrease of the SERS signal subsequently was mainly due to the following two reasons: (i) decreasing gap distance to the sub-nanometer scale could further cause quantum effects which would significantly influence electromagnetic field enhancements and lead to a decrease of the SERS EF and efficiency of conversion reaction.³⁵ (ii) Change of the medium's refractive index would also affect the SERS EF and frequency of the localized SPR according to the Mie theory.³⁶

In summary, a novel efficient strategy for observing dynamic control of the interparticle spacing of nanoparticles in a 2D plane was realized simply by a self-volatilization approach with the nanoparticles. Relationships between the SERS effect, as well as SPR catalytic efficiency and gap distance, were studied theoretically and experimentally. Both SERS intensity and SPR catalytic efficiency increased due to the decrease in interparticle spacing, and this showed considerable catalytic efficiency in some surface reactions with this strategy. This strategy is expected to further provide a significant method to understand the enhancement mechanisms of SERS and to offer an alternative approach for improving SPR catalytic efficiency.

The authors gratefully acknowledge financial support from the Nature Science Foundation of China (21473128 and 21673152),

the National Instrumentation Program (2011YQ031240402), and Priority Academic Program Development of Jiangsu Higher Education Institutions (PAPD).

Notes and references

- R. H. Ritchie, *Phys. Rev.*, 1957, **106**, 874–881.
- A. Hartstein, J. R. Kirtley and J. C. Tsang, *Phys. Rev. Lett.*, 1980, **45**, 201–204.
- M. Fleischmann, P. J. Hendra and A. J. McQuillan, *Chem. Phys. Lett.*, 1974, **26**, 163–166.
- T. Liebermann and W. Knoll, *Colloids Surf., A*, 2000, **171**, 115–130.
- S. M. Nie and S. R. Emory, *Science*, 1997, **275**, 1102–1106.
- K. Kneipp, Y. Wang, H. Kneipp, L. T. Perelman, I. Itzkan, R. Dasari and M. S. Feld, *Phys. Rev. Lett.*, 1997, **78**, 1667–1670.
- K. A. Willets and R. P. Van Duyne, *Annu. Rev. Phys. Chem.*, 2007, **58**, 267–297.
- C. D. Lindstrom and X. Y. Zhu, *Chem. Rev.*, 2006, **106**, 4281–4300.
- Y. F. Huang, H. P. Zhu, G. K. Liu, D. Y. Wu, B. Ren and Z. Q. Tian, *J. Am. Chem. Soc.*, 2010, **132**, 9244–9246.
- B. Dong, Y. R. Fang, L. X. Xia, H. X. Xu and M. T. Sun, *J. Raman Spectrosc.*, 2011, **42**, 1205–1206.
- S. Mukherjee, F. Libisch, N. Large, O. Neumann, L. V. Brown, J. Cheng, J. B. Lassiter, E. A. Carter, P. Nordlander and N. J. Halas, *Nano Lett.*, 2013, **13**, 240–247.
- Y. Zong, Q. H. Guo, M. M. Xu, Y. X. Yuan, R. N. Gu and J. L. Yao, *RSC Adv.*, 2014, **4**, 31810–31816.
- S. K. Cushing and N. Q. Wu, *J. Phys. Chem. Lett.*, 2016, **7**, 666–675.
- Y. Fang, N. H. Seong and D. D. Dlott, *Science*, 2008, **321**, 388–392.
- H. X. Xu, J. Aizpurua, M. Käll and P. Apell, *Phys. Rev. E: Stat. Phys., Plasmas, Fluids, Relat. Interdiscip. Top.*, 2000, **62**, 4318–4324.
- H. L. Liu, Y. D. Sun, Z. Jin, L. B. Yang and J. H. Liu, *Chem. Sci.*, 2013, **4**, 3490–3496.
- J. H. Tian, B. Liu, X. L. Li, Z. L. Yang, B. Ren, S. T. Wu, N. J. Tao and Z. Q. Tian, *J. Am. Chem. Soc.*, 2006, **128**, 14748–14749.
- Y. Lu, G. L. Liu and L. P. Lee, *Nano Lett.*, 2005, **5**, 5–9.
- X. M. Qian, J. Li and S. M. Nie, *J. Am. Chem. Soc.*, 2009, **131**, 7540–7541.
- P. Taladriz-Blanco, N. J. Buurma, L. Rodríguez-Lorenzo, J. Pérez-Juste, L. M. Liz-Marzán and P. Hervés, *J. Mater. Chem.*, 2011, **21**, 16880–16887.
- L. B. Yang, P. Li, H. L. Liu, X. H. Tang and J. H. Liu, *Chem. Soc. Rev.*, 2015, **44**, 2837–2848.
- R. H. Que, M. W. Shao, S. J. Zhuo, C. Y. Wen, S. D. Wang and S. T. Lee, *Adv. Funct. Mater.*, 2011, **21**, 3337–3343.
- Q. H. Guo, C. J. Zhang, C. Wei, M. M. Xu, Y. X. Yuan, R. A. Gu and J. L. Yao, *Spectrochim. Acta, Part A*, 2016, **152**, 336–342.
- Q. H. Guo, M. M. Xu, Y. X. Yuan, R. A. Gu and J. L. Yao, *Langmuir*, 2016, **32**, 4530–4537.
- Y. J. Li, W. J. Huang and S. G. Sun, *Angew. Chem., Int. Ed.*, 2006, **45**, 2537–2539.
- M. A. Mahmoud and M. A. El-Sayed, *Nano Lett.*, 2009, **9**, 3025–3031.
- K. B. Biggs, J. P. Camden, J. N. Anker and R. P. Van Duyne, *J. Phys. Chem. B*, 2009, **113**, 4581–4586.
- H. L. Liu, Z. L. Yang, L. Y. Meng, Y. D. Sun, J. Wang, L. B. Yang, J. H. Liu and Z. Q. Tian, *J. Am. Chem. Soc.*, 2014, **136**, 5332–5341.
- Y. F. Huang, M. Zhang, L. B. Zhao, J. M. Feng, D. Y. Wu, B. Ren and Z. Q. Tian, *Angew. Chem., Int. Ed.*, 2014, **53**, 2353–2357.
- H. Yang, L. Q. He, Y. W. Hu, X. H. Lu, G. R. Li, B. J. Liu, B. Ren, Y. X. Tong and P. P. Fang, *Angew. Chem., Int. Ed.*, 2015, **54**, 11462–11466.
- Y. F. Huang, D. Y. Wu, H. P. Zhu, L. B. Zhao, G. K. Liu, B. Ren and Z. Q. Tian, *Phys. Chem. Chem. Phys.*, 2012, **14**, 8485–8497.
- M. T. Sun, Y. Z. Huang, L. X. Xia, X. W. Chen and H. X. Xu, *J. Phys. Chem. C*, 2011, **115**, 9629–9636.
- E. Z. Tan, P. G. Yin, T. T. You and L. Guo, *J. Raman Spectrosc.*, 2013, **44**, 1200–1203.
- X. J. Liu, L. H. Tang, R. Niessner, Y. B. Ying and C. Haisch, *Anal. Chem.*, 2015, **87**, 499–506.
- J. Zuloaga, E. Prodan and P. Nordlander, *Nano Lett.*, 2009, **9**, 887–891.
- I. Alessandri and J. R. Lombardi, *Chem. Rev.*, 2016, **116**, 14921–14981.